Unveiling the origins and transport processes of radioactive pollutants downstream from a former U-mine site using isotopic tracers and U-238 series disequilibrium

Tingting Geng, Arnaud Mangeret, Olivier Péron, David Suhard, Josselin Gorny, Louise Darricau, Mathieu Le Coz, Nicolas Ait-Ouabbas, Karine David, Christophe Debayle, et al.

Journal of Hazardous Materials 472 (2024) 134416

Contents lists available at ScienceDirect

Journal of Hazardous Materials

journal homepage: www.elsevier.com/locate/jhazmat

Unveiling the origins and transport processes of radioactive pollutants downstream from a former U-mine site using isotopic tracers and U-238 series disequilibrium

Tingting Geng [a,b], Arnaud Mangeret [b], Olivier Péron [a], David Suhard [b], Josselin Gorny [b], Louise Darricau [b], Mathieu Le Coz [b], Nicolas Ait-ouabbas [b], Karine David [a], Christophe Debayle [b], Pascale Blanchart [b], Gilles Montavon [a], Alkiviadis Gourgiotis [b,*]

[a] Laboratoire SUBATECH, UMR 6457, IMT Atlantique/Université de Nantes/CNRS/IN2P3, 4, rue Alfred Kastler, Nantes 44307, France
[b] Institut de Radioprotection et de Sûreté Nucléaire, PSE-ENV/SPDR/LT2S, LETIS, USDR, PSE-SANTE/SESANE/LRSI, Fontenay-aux-Roses F-92260, France

HIGHLIGHTS

- U-Pb isotopic tracing efficiently identified U-mining input in the environment.
- Pitchblende and torbernite exhibit high radiogenic Pb signature.
- Parsonsite lacks radiogenic Pb signature due to its high natural Pb content.
- SIMS analysis confirm the presence of pitchblende and neoformed U-bearing phases.
- U-series disequilibrium highlights U and Ra mobilities in the wetland.

GRAPHICAL ABSTRACT

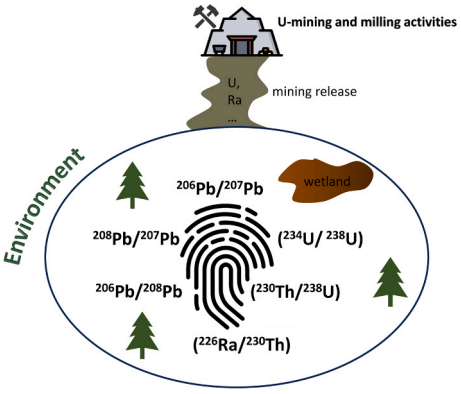

ARTICLE INFO

Keywords:
Pb stable isotopes
U-series disequilibrium
U-contaminated environment
Uranium mines

ABSTRACT

High U concentrations (reaching up to 14,850 mg · kg^{-1}), were determined in soils and sediments of a wetland downstream of a former U mine in France. This study aims to identify the origin of radioactive contaminants in the wetland by employing Pb isotope fingerprinting, ($^{234}U/^{238}U$) disequilibrium, SEM, and SIMS observations. Additionally, information about U and ^{226}Ra transport processes was studied using U-238 series disequilibrium. The results of Pb fingerprinting highlighted inherited material inputs of different U-mines with mainly two types of U-ores: i) pitchblende (UO_2), and ii) parsonsite ($Pb_2(UO_2)(PO_4)_2$). Moreover, significant disequilibrium of ($^{230}Th/^{238}U$) and ($^{226}Ra/^{230}Th$) activity ratios highlighted the mobility of ^{238}U and ^{226}Ra in the wetland, primarily driven by the water table fluctuations. Finally, this work uncovered a limitation of Pb isotope fingerprinting in the case of parsonsite materials, as the high natural Pb content of this mineral may hide the uranogenic Pb signature in the samples.

* Corresponding author.
E-mail address: alkiviadis.gourgiotis@irsn.fr (A. Gourgiotis).

https://doi.org/10.1016/j.jhazmat.2024.134416
Received 4 December 2023; Received in revised form 8 April 2024; Accepted 23 April 2024
Available online 26 April 2024

1. Introduction

The expansion of global U mining industry since the early twentieth century, driven by the increasing demand for the nuclear industry, has resulted in U contamination downstream of mining sites, particularly wetlands [1-7]. For instance, the average U concentration of upper continental crust is around 2.8 mg · kg^{-1} [8]. The wetland adjacent to former U mine tailings in Germany exhibited an accumulation of 7500 mg · kg^{-1} U [5], and higher U levels of up to 14,000 mg · kg^{-1} were also observed in a wetland downstream of a former U mine in France (Limousin region) [7]. Natural accumulation of U in mountainous regions due to weathering and erosion of uraniferous rocks, such as granites (U concentration: 2.2–6.1 mg · kg^{-1}), can also lead to comparable levels of U to that of mining contamination [9-12]. The natural U accumulation in wetland reached up to 10,000 mg · kg^{-1} in organic-rich wetlands in USA [13]. Identifying the potential sources of radioactive contamination offers vital insights for the decision-making process, effective management, and remediation of contaminated soils and/or sediments.

Pb source identification has also been employed as an effective tool for tracing the impact of U mining activities in the environment for decades [14,15,1,2,4,16]. This is based on the Pb isotopic composition contrast between U-ores and natural Pb sources. Natural Pb in the Earth's crust comprises ^{204}Pb (1.1 %), ^{206}Pb (25.4 %), ^{207}Pb (21.1 %), and the most abundant isotope ^{208}Pb (52.4 %), due to the higher concentration of ^{232}Th in the bedrock compared to that of U. Among them, ^{206}Pb, ^{207}Pb, and ^{208}Pb are final decay products of ^{238}U, ^{235}U, and ^{232}Th. In U-ores, the high U and low Th content lead to the high production of radiogenic Pb, notably ^{206}Pb and ^{207}Pb compared to that of ^{208}Pb [16, 17]. Hereafter, the term radiogenic refers to Pb produced by the U-decay in U-ores. Tailings and materials contaminated by U-mining activities including soils, sediments, groundwater, and mussels, inherit the Pb isotopic signature of U-ores exhibiting higher $^{206,\ 207}$Pb/ ^{208}Pb ratios compared to natural materials [14,18,19,2]. As a result, environmental samples affected by uranium mining activities exhibit elevated Pb radiogenic isotope signatures, significantly differing from those found in environmental analyses focused on identifying sources of heavy metal pollutants [20,21].

Wetlands could also act as secondary U sources which release U and its decay products to surroundings. Hence, their mobility has also been studied to predict their future fate and environmental impacts [22-24]. Recent mobility tracing of U and Ra has relied on activity ratios of radionuclides in ^{238}U decay series, particularly (^{230}Th/^{238}U), (^{226}Ra/^{230}Th), and (^{234}U/^{238}U). When these activity ratios are equal to 1, this means that ^{238}U decay nuclides are in a secular equilibrium over a period exceeding 6 half-lives of the shorter-lived nuclide. However, the different physicochemical properties between radionuclides, and the alpha recoil effect can lead to the radioactive disequilibrium. As ^{230}Th exhibits low mobility [25,26], the deviation of (^{230}Th/^{238}U) and (^{226}Ra/^{230}Th) underlines a gain or loss of ^{238}U and ^{226}Ra. Additionally, the disequilibrium of (^{234}U/^{238}U) activity ratios reflect the fluid-rock interaction due to the alpha recoil effect, which plays a fundamental role in the fractionation of radionuclides. During α decay from ^{238}U, the daughter nuclide ^{234}Th is generated and forced in the opposite direction of the α particle ones, leaving the host U-containing mineral. Oxygen atoms are also accumulated in front of ^{234}Th and then lead to a subsequent oxidation of ^{238}U(IV) to ^{234}U(VI). This oxidation process promotes the preferential release of the ^{234}U into the solution [27] and thereby a disequilibrium of (^{234}U/^{238}U) activity ratio in sediments [28-30]. Recent works have demonstrated that this process, before U-ore extraction, during the contact of U-ore with gangue mineral phases, can lead to high (^{234}U/^{238}U) activity ratios in the U-tailing materials [31–33]. This specific ratio can be combined with stable lead isotopes to highlight tailing material dissemination in the environment [34].

This study is focused on the source tracing of historical radioactive contamination in the context of a U-contaminated wetland located in the vicinity of the former U mine at Rophin in France. This site, which is part of the research program of the Zone Atelier Territoire Uranifère (ZATU), has a complex U mining history with a mixed presence of various U-ores [4] and serves as an experimental U-contaminated wetland in France, dedicated to multifaceted investigations regarding the environmental impacts of irradiation [35-37,4]. Building on previous research [4], the first objective of this study is to precisely identify the different sources responsible for the radioactive contamination, correlating with the distinct mining phases in the site's history. The second objective of this study is to have a deeper qualitative comprehension of the radionuclide mobility in the wetland, notably U and Ra. A variety of geochemical approaches, including Pb isotopic tracing, radioactive disequilibrium of ^{238}U, and SEM and SIMS observations were employed to answer these questions.

2. Methods and materials

2.1. Study site and mining history

The former U mine of Rophin is situated in the Massif Central (Puy-de-Dôme, France) (Fig. 1a, b). It was in operation from 1949 to 1952 as part of the Western Lachaux ores [35,36,4]. The ore bodies of western Lachaux sector are hosted by the by coarse-grained peraluminous granite of the alkaline type. The main U veins, extending to Etang de Reliez, Reliez, Gagnol and Bancherelle, are charaterized by large-crystal smoky quartz. The dominated U mineral here is parsonsite ($Pb_2(UO_2)(PO_4)_2$), with less torbernite ($Cu(UO_2)_2(PO_4)_2$) and autunite ($Ca(UO_2)_2(PO_4)_2$). Other accessory minerals include pyromorphite $Pb_5(PO_4)_3Cl$, galena (PbS) [35,38].

A mechanical ore-washing plant was constructed on-site for processing U-ores of Rophin in 1948. Wastewater was discharged into basins and then directed to an effluent that flows into the stream 'Le Gourgeat' [4] (Fig. 1b). An experimental chemical extraction with pressurized Na_2CO_3 was initially processed on a batch of 90 tons of ore (pitchblende (UO_2)) originating from Bois Noirs in 1950, another U mine located approximately 20 kilometers east of the Lachaux region [39,35,4]. Since the extraction performance was inadequate, this procedure was abandoned and replaced with mechanical processing involving crushing, grinding, and washing.

Currently, over 30,000 tons of mining and U mill tailings are stored at the Rophin site, which is designated as Registered environmental facility (ICPE: Installation classée pour la protection de l'environnement) (Fig. 1b). The wetland, located at the confluence of the ICPE drainage stream and the Gourgeat, is seasonally flooded and characterized by the highest recorded dose rate, which can reach levels of up to 2,000 nSv · h^{-1}.

2.2. Samples collection and preparation

Three U-ore samples were collected close to Rophin and Etang de Reliez (Fig. 1a): parsonsite ($Pb_2(UO_2)(PO_4)_2$), torbernite ($Cu(UO_2)_2(PO_4)_2$), and pitchblende (UO_2) (Fig. SI-1). It is worthy noted that pitchblende is not the local mineralisation of Rophin. This mineral, originated from Bois Noirs, can be found at Rophin site due to its chemical processing in 1950s (see section 2.1).

According to dose rate variations in the area, soil cores were sampled from sites exhibiting anomalies in dose rate, as well as from areas where the dose rate aligned with the local background (Fig. 1b). A Russian

corer (Eijkelkamp®) of 100 cm length and 5 cm diameter was used for sampling in October 2021.

Soil core C4 was collected from the banks of a trench that was not affected by mine drainage. All the other soil cores were sampled upstream, downstream and within the wetland (Fig. 1b). Subsamples were collected at different depths and preserved in 50 mL Falcon tubes. Once back in the laboratory, these samples were frozen in the freezer at -20 ˚C. Then, these samples were manually crushed in an agate mortar and pestle after 24–48 h of drying in a laboratory oven set to 100˚C for chemical analysis.

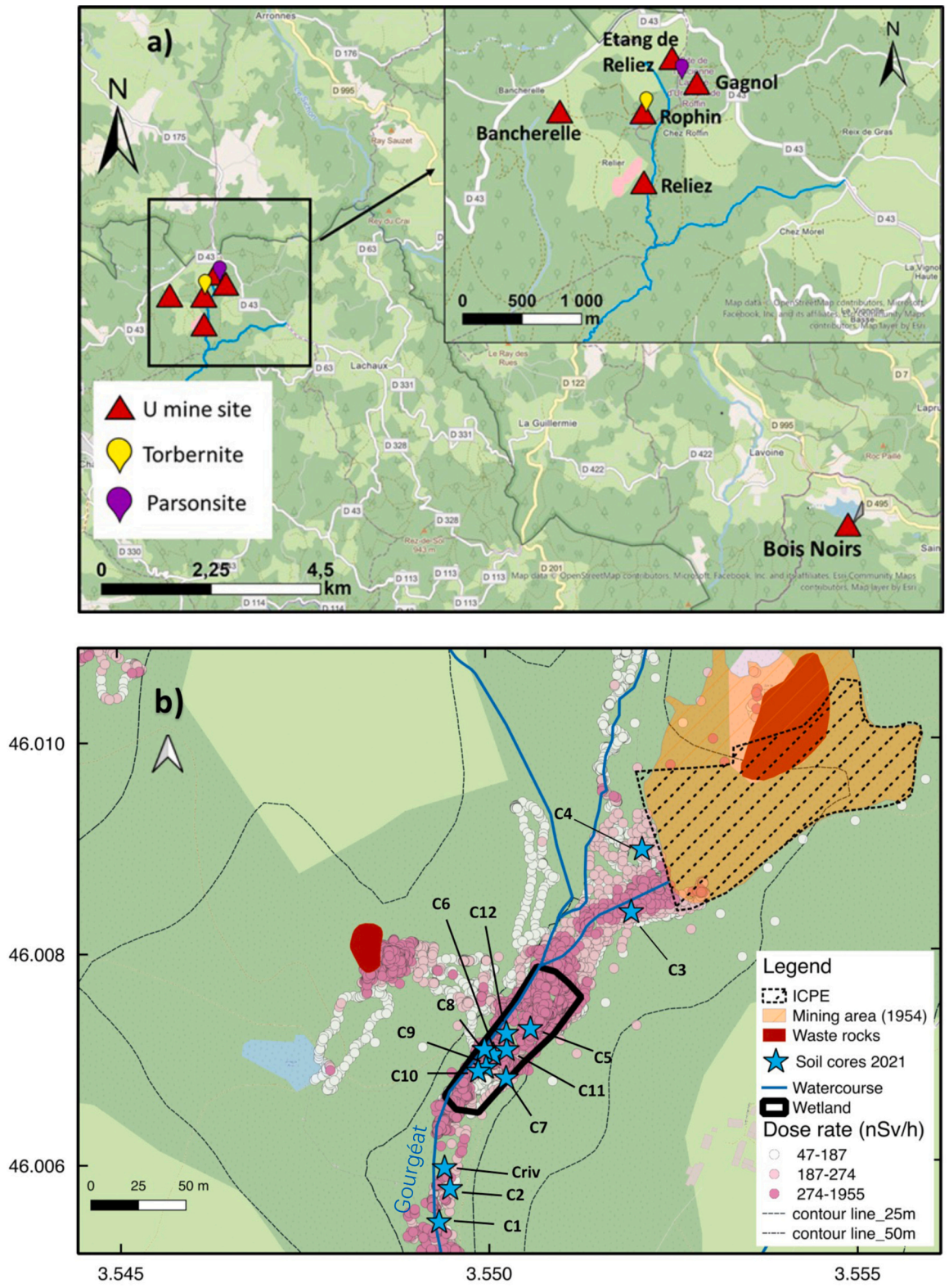

Fig. 1. (a) The former U mine sites of Lachaux: Gagnol, Rophin, Etang de Reliez, Bancherelle, Reliez, and Bois Noir Limouzat. (b) Downstream overview of the former U mine site-Rophin (ICPE nowadays) and sampling sites.

2.3. Core description

Four distinct soil layers were identified: a surface organic-rich layer (L1), an underlying orange sandy layer (L2), a whitish clayey layer (L3), and a paleosol layer (L4). The organic carbon content (C_{org}), water content, and a brief description of each layer are summarized in Table SI-1. The surface layer (L1) primarily consists of leaf litter, roots, and humus. This layer is characterized by a high C_{org} content (11–31 %) and a significant water content (68–83 %). The orange sandy layer (L2), located beneath L1, exhibits a sandy/silt texture and the lowest water content (14–48 %) and C_{org} (0.1–1.8 %). The whitish clayey layer (L3) contained 21–76 % water and 0.1–14 % C_{org} contents. This layer was suggested to be closely associated with the discharge of former U processing waters [4,40]. Lastly, the paleosol layer L4, situated at the deepest level within the profiles, consists of small fragmented bedrocks and roots. It has a higher C_{org} content than L2 and L3 (1–15 %) while its water content is similar to that of L3 (Fig. 2).

These soil cores visually showed a spatial heterogeneity as the depth and the thicknesses of soil layers vary across cores. It is worth noting that the distribution of L2 and L3 layers is particularly heterogeneous (Fig. SI-2).

2.4. Elemental, Pb isotopes, and U-Th analysis

About 50 mg of solid samples were dissolved in a mixed concentrated acid of 1 mL HF (47–51 %, VWR ultrapure®) and 1 mL HNO_3 (67%, VWR ultrapure®) in Savillex® PFA vials for digestion into solution. The mixture was then evaporated to dryness. To dissolve the fluoride residue, ten drops of $HClO_4$ (~ 300 μL) were added, and the mixture was evaporated to dry at 160 °C [34,2,41-43]. The dry residue was dissolved in 5 mL of 3 mol · L^{-1} HNO_3. This solution was used for elemental, Pb isotopes and U-Th analysis. More details about the analytical protocols can be found in the Supplementary Information.

2.5. Gamma spectrometry analysis

The radiometric analyses of ^{238}U, ^{226}Ra, and ^{230}Th were performed using gamma spectrometry equipped with an HPGe well-type detector (GWL-220–15, ORTEC®) at the LUTECE platform (IRSN). The counting times were 24–48 h. About 1–2 g samples were sealed with 0.5 cm width

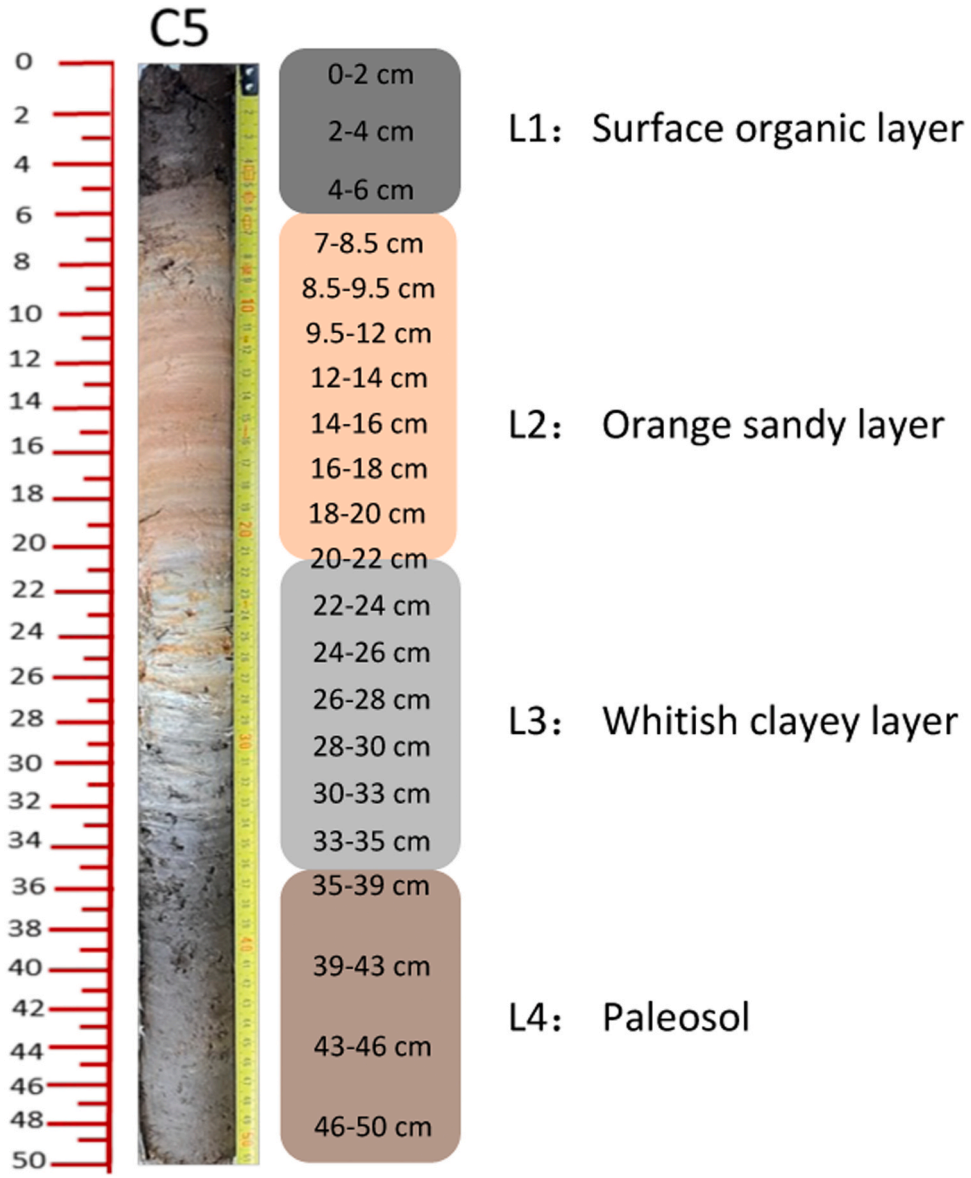

Fig. 2. A typical soil core C5 (left), sampled within the wetland, downstream of the former Rophin site (ICPE) and an illustration profile (right) of the main soil layers and observed in these cores, with depth of samples.

of Parafilm® and 0.5 cm width of a non-radioactive resin for polyethylene materials in air-tight 5 mL plastic geometries, preventing the loss of ^{222}Rn. The determination of ^{238}U, ^{226}Ra, and ^{230}Th was performed respectively according to the gamma ray peaks of ^{234}Th (63.29 keV), ^{214}Pb (295.22 and 351.93 keV), and ^{230}Th (67.67 keV). A secular equilibrium after 3 weeks was obtained between ^{226}Ra and its daughter isotopes ^{214}Pb and ^{214}Bi. The gamma detector was calibrated using international IAEA standards (IAEA-RGU1, IAEA-RGTh1). The detailed measurement procedures were reported in previous studies [34, 3,44]. Gamma quality control was performed using in-house standards of IRSN (with sediment and soil matrix).

2.6. SEM analysis

The identification of Pb and U-bearing phases within selected soil samples was performed using a Scanning Electron Microscope (SEM), specifically the Hitachi S3500N, coupled to two Brücker 5030 Flash Silicon Drift Detectors (SDD) at the LUTECE platform (IRSN). Sample preparation involved the following steps: the soil samples were first embedded in resin (Epoxy, Struers) to stabilize the structure, then polished to achieve a smooth surface suitable for analysis. Subsequently, the samples were coated with a thin carbon layer to prevent charging effects that could interfere with the electron imaging process.

SEM observations were carried out using both Secondary Electron (SE) and Back Scattered Electron (BSE) detectors, operating at an accelerating voltage ranging from 15 to 25 keV. The chemical composition of the samples was analyzed using Energy Dispersive X-ray Spectroscopy (EDS). This technique allows for precise determination of the distribution and quantification of elements within the analyzed phases.

2.7. SIMS imaging

The secondary Ion Mass Spectrometers (SIMS) were used to accurately localized the radiogenic Pb within U-bearing particles at the grain scale. The analysis were carried out using a CAMECA IMS 7 F-E7 instrument. The carbon-coated sample (C5, 8.5–9.8 cm), prepared for SEM analysis, was directly introduced into the analysis chamber of the instrument under a pressure condition of 1.9×10^{-9} mbar. The analysis used a 5 nA, 15 kV $^{\dagger}_{2}O^{+}_{2}$ primary ion beam directed onto an area of approximately 1 cm, scanning the region of interest with a 250 μm $\times$ 250 μm raster. Positively charged secondary ions or molecules generated were subsequently accelerated at 10 kV into the mass spectrometer. Measurements were performed with a mass resolution of 400 through ion counting in mono-collection mode, resulting in the sequential production of an image with a lateral resolution of around 1.5 μm. Before each analysis, a 2-minute pre-sputtering step was performed using a 500 nA primary ion beam. This process serves to eliminate the carbon layer on the sample surface, ensuring the primary ion beam reaches the sample surface and renders it conductive. This conductivity enables the emission of secondary ions during the subsequent analysis. The analysis includes 500 integration cycles, each lasting 10 s for $^{206}Pb^{+}$, $^{207}Pb^{+}$, $^{208}Pb^{+}$, and $^{238}U^{16}O^{+}$, and 1 s for $^{63}Cu^{+}$ and $^{28}Si^{+}$. To calibrate the mass of the instrument, a Pb-rich metal plate with a common Pb isotopic signature was employed for Pb and torbernite was used for Cu.

3. Results and discussion

3.1. U, Pb, ^{232}Th concentrations and ^{230}Th, ^{226}Ra activities in the wetland

The patterns of U, Pb, ^{232}Th, ^{226}Ra, and ^{230}Th levels across different soil layers are illustrated in Fig. 3. Notably, ^{232}Th concentration remains stable throughout the soil profile (11–33 mg · kg^{-1}), while the concentrations of other radionuclides show important variations. The detailed data is provided in Table SI-2, SI-3, SI-4, SI-5, SI-6, SI-7.

Considered as the local geochemical background, the paleosol layer

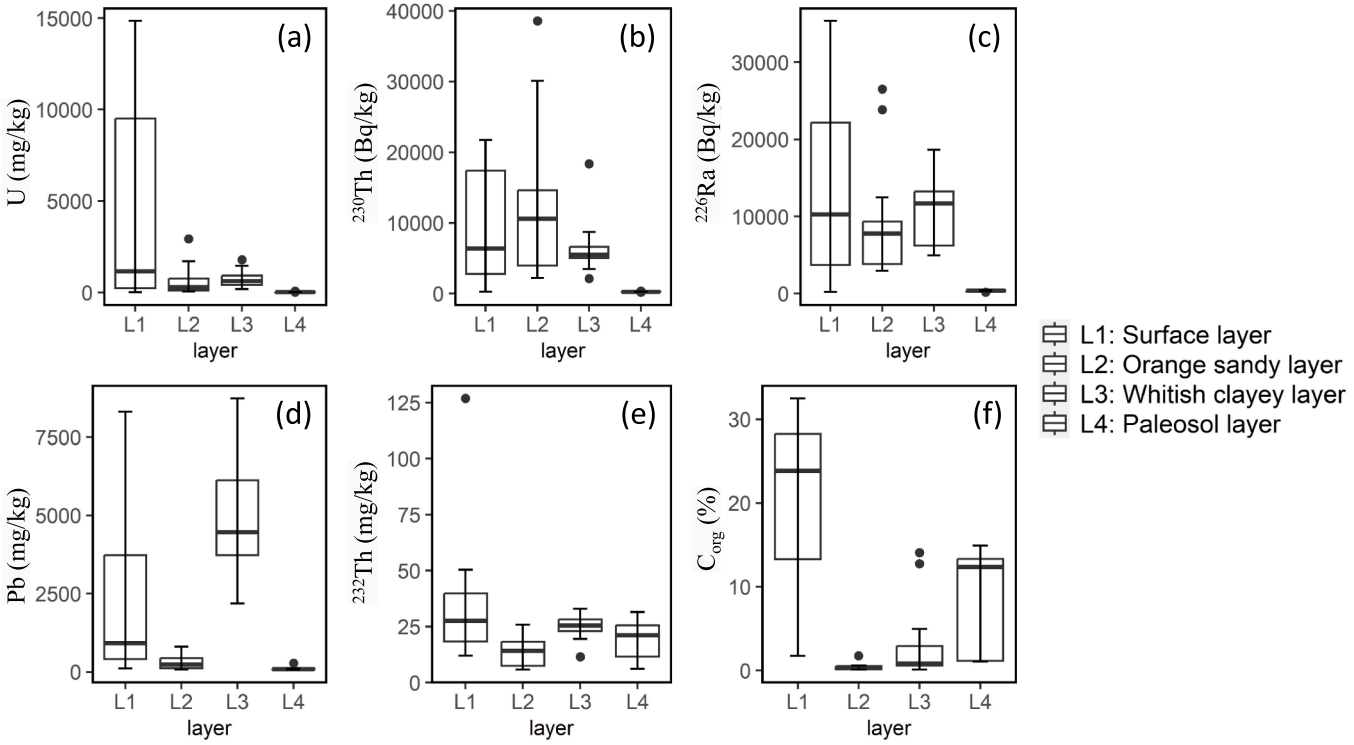

Fig. 3. Box-plots illustrating the distribution of (a) C_{org}, (b) U, (c) Pb, (d) ^{232}Th contents, as well as (e) ^{230}Th and (f) ^{226}Ra activities across soil layers (L1-L4). L1: samples collected in soil core C1, C5, C9, C12; L2: samples from core C1, C5, C6, C10; L3: samples from core C1, C3, C5, C6, C10, Criv; L4: samples collected from core C1, C3, C4, C5.

(L4) reveals an average U concentration of 35 mg · kg^{-1} and Pb concentration of 141 mg · kg^{-1}. Additionally, ^{226}Ra activity averages 266 Bq · kg^{-1} , while that of ^{230}Th remain below 276 Bq · kg^{-1}.

By comparing with the local geochemical reference L4, the layers L3, L2, and L1 exhibit higher U, Pb, ^{226}Ra and ^{230}Th levels. For the layer L3, this layer exhibits significantly elevated U and Pb concentrations, with median values of 621 mg · kg^{-1} and 4,492 mg · kg^{-1}. The activity levels of ^{226}Ra and ^{230}Th are also high, with median values of 11,701 Bq · kg^{-1} and 5,483 Bq · kg^{-1}. In contrast to L3, U and Pb concentrations significantly drop in layer L2, falling to 285 mg · kg^{-1} and 240 mg · kg^{-1}. However, the ^{226}Ra and ^{230}Th activities remain at high levels (median: 7,797 Bq · kg^{-1} for ^{226}Ra and 10,588 Bq · kg^{-1} for ^{230}Th, respectively). This probably suggests a loss of U in this layer while its decay products ^{226}Ra and ^{230}Th, which are less mobile than U, remain relatively concentrated. The mobility of these radionuclides will be detailed in section 3.3. Layer L1 stands out prominently due to its notably high median concentrations of U (1,159 mg · kg^{-1}) and Pb (921 mg · kg^{-1}), as well as the median radioactivity for ^{226}Ra (10,261 Bq · kg^{-1}) and ^{230}Th (6,404 Bq · kg^{-1}). Furthermore, a noteworthy extreme local accumulation is observed in core C5, where U concentration reaches up to 14,850 mg · kg^{-1}, Pb up to 8,310 mg · kg^{-1}, and ^{226}Ra up to 35,368 Bq · kg^{-1}. The ^{230}Th activity in this layer of C5 is also high, up to 21,724 Bq · kg^{-1}. Comparable elevated levels (14,000 mg·kg^{-1} of U, 29,550 Bq · kg^{-1} of ^{226}Ra, and 37,633 Bq · kg^{-1} of ^{230}Th) were already reported in organic layer of U-contaminated wetlands downstream of former U mine sites in France [7]. The presence of substantial organic matter in layer L1 is likely responsible for these observations, as these elements are known to have a strong affinity for organic matter, leading to their retention within it [25,36,45].

3.2. Identification of the U sources in the downstream wetland

3.2.1. Potential U sources at Rophin

The chemical composition analyses of three U-rich ore samples are displayed in Fig. 4 along with their SEM images.

- The U-ore sample of Etang de Reliez contains mainly Pb (37 %), P (31 %), and U (18 %) (Fig. 4a). The atomic content is consistent with the chemical composition of Rophin parsonsite $Pb_2(UO_2)(PO_4)_2$ determined previously by Branche et al. [46].
- The U-ore sample from a quartz vein at Rophin, contains mostly U (28 %), P (23 %), Si (19 %), Al (14 %), Cu (13%), and Fe (2.5 %) (Fig. 4b). Based on its atomic ratios of U/Cu (2.15), U/P (1.22), and P/Cu (1.77), U-rich minerals were suggested to be torbernite Cu $(UO_2)_2(PO_4)_2$.

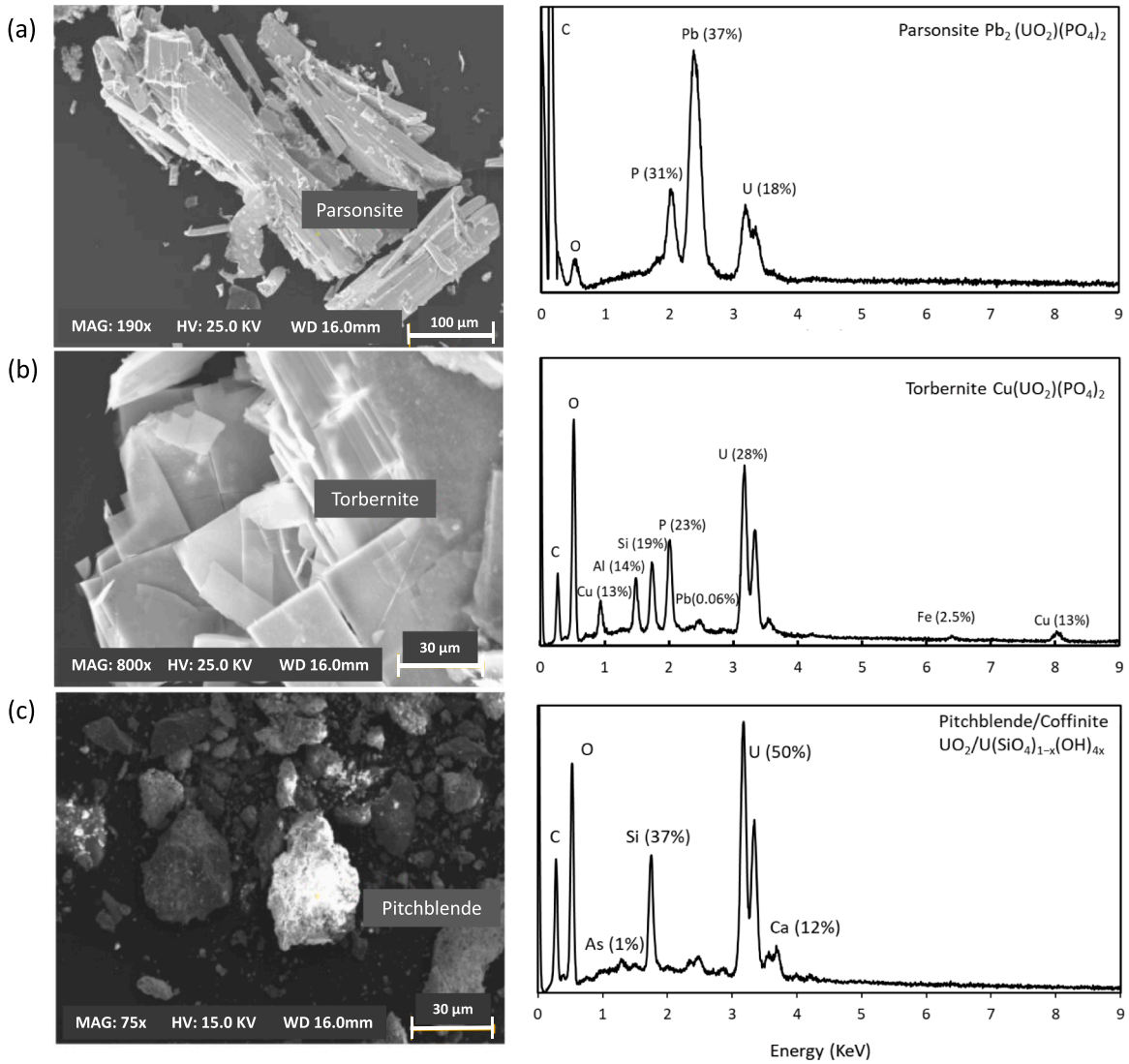

Fig. 4. The SEM-EDX observations and the atomic percentage of elements presented in (a) parsonsite, (b) torbernite, and (c) pitchblende/coffinite.

- The U-ore sample collected at the dump of Rophin consists of U (50 %), Si (37 %), along with Ca (12 %), As (1 %). This suggests that this U-ore is probably pitchblende (UO_2) or coffinite ($USiO_4$). As the Rophin site lacks pitchblende/coffinite, and according to the mining history, this U-ore probably originated from the Bois Noirs.

3.2.2. Discriminating U sources in the wetland

3.2.2.1. Endmembers. Soils and sediments impacted by U-mine discharges normally show higher ratios of $^{206}Pb/^{207}Pb$ (ex. 1.21–8.92), and lower ratios of $^{208}Pb/^{207}Pb$ (ex. 0.26–2.49) compared to the bedrocks [14,47,48]. This feature enables the discrimination between natural and U-mining inputs.

A binary mixing model, involving U sources (U-ores) and natural sources (local background) as two endmembers, allows highlighting the U-sources of soils and sediments in the wetland. This model is represented in the three-isotope Pb diagram (Fig. 5). The U-ore exhibits radiogenic Pb signature, as confirmed by our observations of torbernite ($^{206}Pb/^{207}Pb \sim 3.65$) and pitchblende ($^{206}Pb/^{207}Pb \sim 9.60$) while the natural source shows natural Pb isotopic signature ($^{206}Pb/^{207}Pb \sim 1.2$). As can be seen in Fig. 5, Pb isotope ratios fit in the area representing the U-ore deposits in France (dating between 40–300 Ma) [49]. The $^{206}Pb/^{207}Pb$ ratios of these endmembers (pure radiogenic Pb) range from 19.11 to 21.36 and $^{208}Pb/^{207}Pb$ ratio is close to zero (low Th content of U-ores). The alignments of the soil and sediment samples confirm the presence of the U-mining inputs in the wetland and support the three U-ore sources (parsonsite, torbernite and pitchblende). Samples showing radiogenic Pb signatures(typically samples of layer L2), highlight the input of U related to pitchblende or/and torbernite. Other samples with an non-radiogenic Pb signature, could either be impacted by former U mining discharges related to the treatment of parsonsite ores or natural Pb input such as Pb-rich mineral.

In fact, a common Pb isotopic signature (Pb from local geological background) is observed in the parsonsite. This can be elucidated by the high Pb content from local geological background (LGB) that has been present since its formation ([Pb] $\sim$ 2 x[U]). As shown in Fig. 6, the radiogenic Pb quantity generated in parsonsite from U-deacay, is insufficient to significantly change its inherent LGB isotope signature, for ages $<$ 30 Ma. With the increase of parsonsite ages, the radiogenic Pb signature becomes more pronounced. This implies a relatively young age for the parsonsite at Rophin ($<$ 30 Ma). Furthermore, this observation underscores the challenge in tracing U-mining sources via Pb isotopes when mixed with high Pb content from LGB. It also implies that

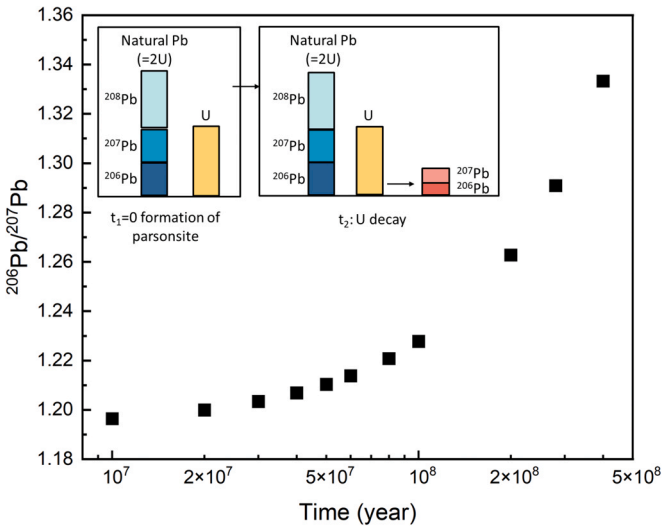

Fig. 6. Model showing the temporal evolution of $^{206}Pb/^{207}Pb$ ratio in parsonsite as a function of time for a system with U and Pb content close to parsonsite stoichiometry at t = 0 ([Pb] = 2[U]). The model was run from 0 to 500 Ma, which largely covers the age of the Rophin mine (French mineralization events from 40–300 Ma [49]). The calculation is based on the equations of Holmes-Houtermans System [50].

soils and sediment samples displaying nonradiogenic Pb signature (e.g. layer L3) can be either impacted by former U mining discharges related to the parsonsite mining and milling activities.

The Pb isotopic signature and the observed radionuclide contents are consistent within a soil layer across varying depths and different soil cores. Thus, the subsequent analysis directly focuses on the most representative soil core C5, located at the center of the wetland.

3.2.2.2. Paleosol layer (L4). Paleosol, characterized by a natural Pb isotopic signature ($^{206}Pb/^{207}Pb = 1.19–1.23$), is considered as the local geochemical background. This ratio aligns with PDAC (Present Day Average Crustal), with $^{206}Pb/^{207}Pb = 1.2$, respectively [51].

3.2.2.3. Whitish clayey layer (L3). In contrast to layer L2, the whitish clayey layer (L3) exhibits $^{206}Pb/^{207}Pb$ ratios ranging from 1.18 to 1.23, corresponding to values between the endmember parsonsite ratio (1.19) and the local background ratio (1.23) (Fig. 4b). Even if the Pb isotope

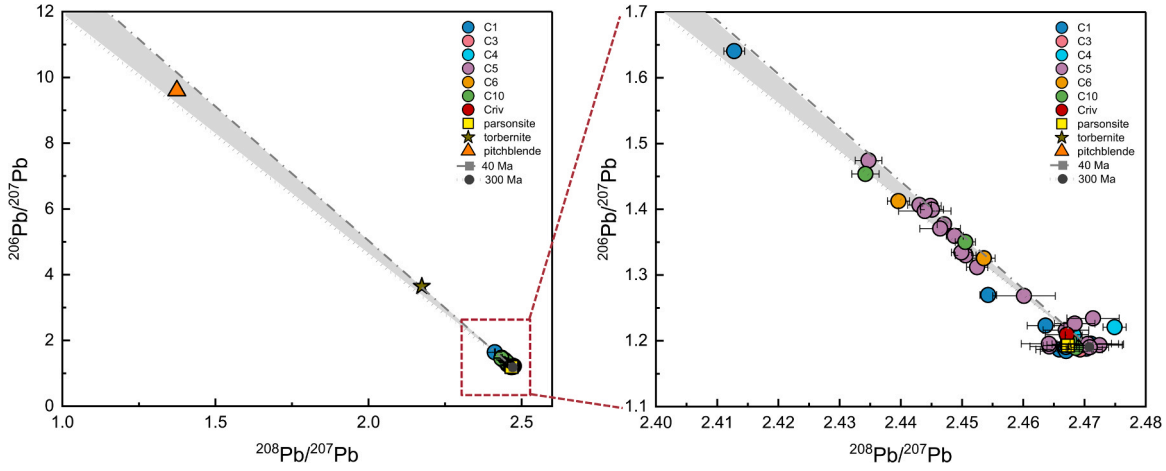

Fig. 5. Pb three-isotope diagram illustrating $^{206}Pb/^{207}Pb$ vs $^{208}Pb/^{207}Pb$, and a detailed zoom-in on the different soil layers (L1, L2, L3, L4) of sampled soil cores and U-ore samples. Data are available in Table SI-5, SI-6 and SI-7. In both sections of the diagram, the dotted lines represent the Pb isotopic composition of U deposits that formed within the specific geological time frame of 40 to 300 million years ago (Ma), corresponding to the age range of U-ore deposits in France. When error bars are not visible, they are included within the data points. All uncertainties are expressed with a coverage factor of k=2.

ratio could not be used to distinguish parsonsite from the local background, high Pb and U concentrations suggested the presence of a mixture containing both. The predominant Pb source between them would control the Pb isotopic signature of this layer. It is highly possible that parsonsite serves as the primary U source, assigned to the mine discharge that occurred during the 1950s, involving the mechanical processing of Rophin and Etang de Reliez parsonsite-rich ores. This assumption is consistent with the previous study of Martin et al. [4], which employed ^{14}C and ^{137}Cs dating methods. The poor efficiency of U milling during this period further reinforces the identification of parsonsite within this layer, as confirmed by SEM analysis (Fig. 7a). Besides, the presence of other minerals inherited from U mineralization, such as pyromorphite (Fig. 7b) which is present at Rophin, provides additional support for our hypothesis.

3.2.2.4. Orange sandy layer (L2). The layer L2 exhibits higher $^{206}Pb/^{207}Pb$ ratios ($^{206}Pb/^{207}Pb$ = 1.27–1.47) and lower $^{208}Pb/^{207}Pb$ ratios ($^{208}Pb/^{207}Pb$ = 2.44–2.46) than the local geochemical background ($^{206}Pb/^{207}Pb$ = 1.22, $^{208}Pb/^{207}Pb$ = 2.47) (Fig. 5b). Similar $^{206}Pb/^{207}Pb$ ratios were found in surface sediments of drainage channels and natural water reservoirs downstream of the former U mine in China (1.25–1.87) [52], the Bertholène mine (1.445–1.547) in France [1], and the Ranger mine area in Australia (1.51–1.80) [53]. Additionally, higher $^{206}Pb/^{207}Pb$ ratios were determined in wetland soils collected downstream of the former mining site of Ty-Gallen in France (up to 10.73) [2], as well as in filtered particles of aerosol particles (1.58–4.00), water (1.18–3.08), and mussels (1.26–2.20) in the U mine area [14-16]. The radiogenic Pb signature observed in layer L2 strongly implies that this layer contains deposits resulting from U mining discharges. Notably, the pitchblende and torbernite, both exhibiting radiogenic Pb signatures, further indicate that these minerals may have served as primary sources of U in this layer.

However, Pb isotopic composition cannot uniquely differentiate the source of U, i.e.,whether it is torbernite of Rophin or the pitchblende of Bois Noirs. To address this limitation, we used $^{206}Pb/^{207}Pb$ and ($^{234}U/^{238}U$) ratios to distinguish the input from the chemical processing of U-ores (pitchblende), as proposed by [34] and depicted in Fig. 8a. The ($^{234}U/^{238}U$) activity ratios of this layer exhibit a slight disequilibrium ranging from 0.999–1.083. Given the mine site history, it was known that U-ores from Bois Noirs were chemically processed at Rophin. Therefore, the radioactive disequilibrium and the radiogenic Pb signature observed in layer L2 serve as evidence of wastewater discharges from the chemical processing of pitchblende derived from the Bois Noirs deposit. Additionally, the layer L2 exhibits a disequilibrium of ($^{230}Th/^{238}U$) activity ratio ranging from 1.44 to 4.4, likely attributable to the ^{238}U extraction during the chemical processing with Na_2CO_3 salts. This is consistent with our assumption and supported by investigations of ($^{230}Th/^{238}U$) activity ratio in U-mill tailings worldwide: ($^{230}Th/^{238}U$) activity ratios ranging from 6.6 to 65 have been observed in Gabon and France, and ratios ranging from 2.5 to 10 have been reported in Australia [34,54] (Fig. 8a).

The weight ratio of [Cu]/[U], as illustrated in Fig. 8c, is also a helpful tracer in identifying potential Cu input associated with the presence of torbernite. However, the potential presence of Cu deposits at Rophin limits the use of this diagram: in fact, [Cu]/[U] ratios are higher than torbernite's stoichiometry, indicating the presence of secondary Cu mineral phases. An example observed by SEM was presented in Figure SI-4.

Various U-bearing phases were identified through SEM and SIMS observations. In Fig. 9 (Area 1), Pb-rich U-bearing phases having a common Pb isotopic signature (Pb from LGB) are shown. The presence of another U-rich particle containing high radiogenic Pb level ($^{206}Pb/^{208}Pb$~9.15), without Cu, confirms the presence of pitchblende from Bois Noirs in this layer (Fig. 9, Area 2). This mixing can explain the lower radiogenic Pb signature identified in this layer in sample bulk analysis compared to the reported values for U-ore/U tailing samples [34,55,16]. Other U-bearing phases such as U-phosphates and Fe-oxides were also observed (Fig. SI-4). These findings are particularly noteworthy as these minerals were also identified in clayed and silty-sand U mill tailings stored underwater at the site of Bois Noirs [22].

3.2.2.5. Surface layer (L1). The surface layer exhibits a slightly radiogenic Pb isotopic signature ($^{206}Pb/^{207}Pb$: 1.27–1.33). This variation indicates the presence of a mining input in the surface layer. However, the origin of this input remains uncertain, as it could be attributed to either the wetland still receiving U (dissolved and particulate phases) from water in the watershed impacted by former U-mining activities [56], or it may be linked to seasonal fluctuations in the water table, resulting in the remobilization of U from the underlying layer to the surface [4,40]. Recent research suggests that the stream 'Gourgeat' continues to receive U releases from the ICPE of Rophin and transport the U in the form of colloids including organic matter and Fe oxides [36, 56]. Such an accumulation mechanism in the wetland has also been similarly described for other U-mining contaminated sites [3,57]. On the other hand, the remobilization of U with water table has also been reported [6], and we will detail it in the section 3.3.

3.3. The mobility of ^{238}U, ^{226}Ra in the profile

Considering the relatively low solubility of Th compared to Ra and U, the activity ratios of ($^{230}Th/^{238}U$) and ($^{226}Ra/^{230}Th$) shed light on the mobility of ^{238}U and ^{226}Ra within the weathering profile [25,58,9]. The data is detailed in the Tab. SI-8, SI-9, SI-10. Fig. 8b illustrates these activity ratios for investigated soil and sediment samples. In both unweathered primary ore and particles, the ($^{230}Th/^{238}U$) and ($^{226}Ra/^{230}Th$) activity ratios are typically close to secular equilibrium, suggesting that the decay products of the ^{238}U chain, including ^{230}Th and ^{226}Ra, are not influenced by migration processes [25]. Any deviations from secular equilibrium reflect U and Ra loss or gain in dissolved forms. Such fluctuations are intricately linked to the geochemical processes that govern the dispersion of U and its decay products. These complex processes include the dissolution of primary U-ore minerals,

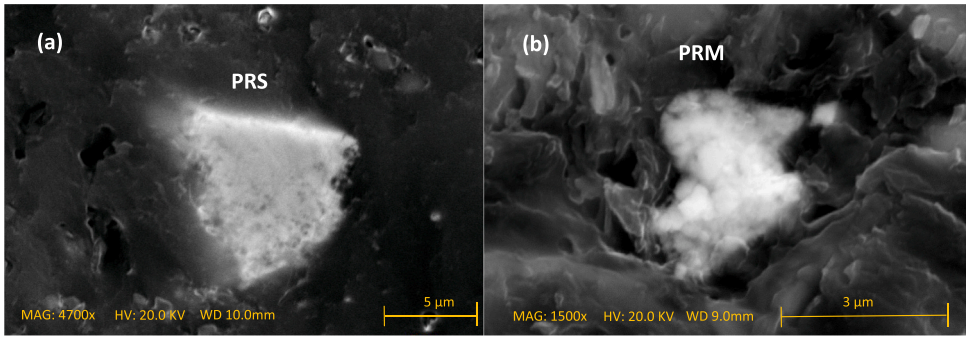

Fig. 7. SEM-SE/BSE characterization of U-bearing phases in the whitish layer L3 of core C5 (30–33 cm): (a) Parsonsite (PRS), (b) Pyromorphite (PRM).

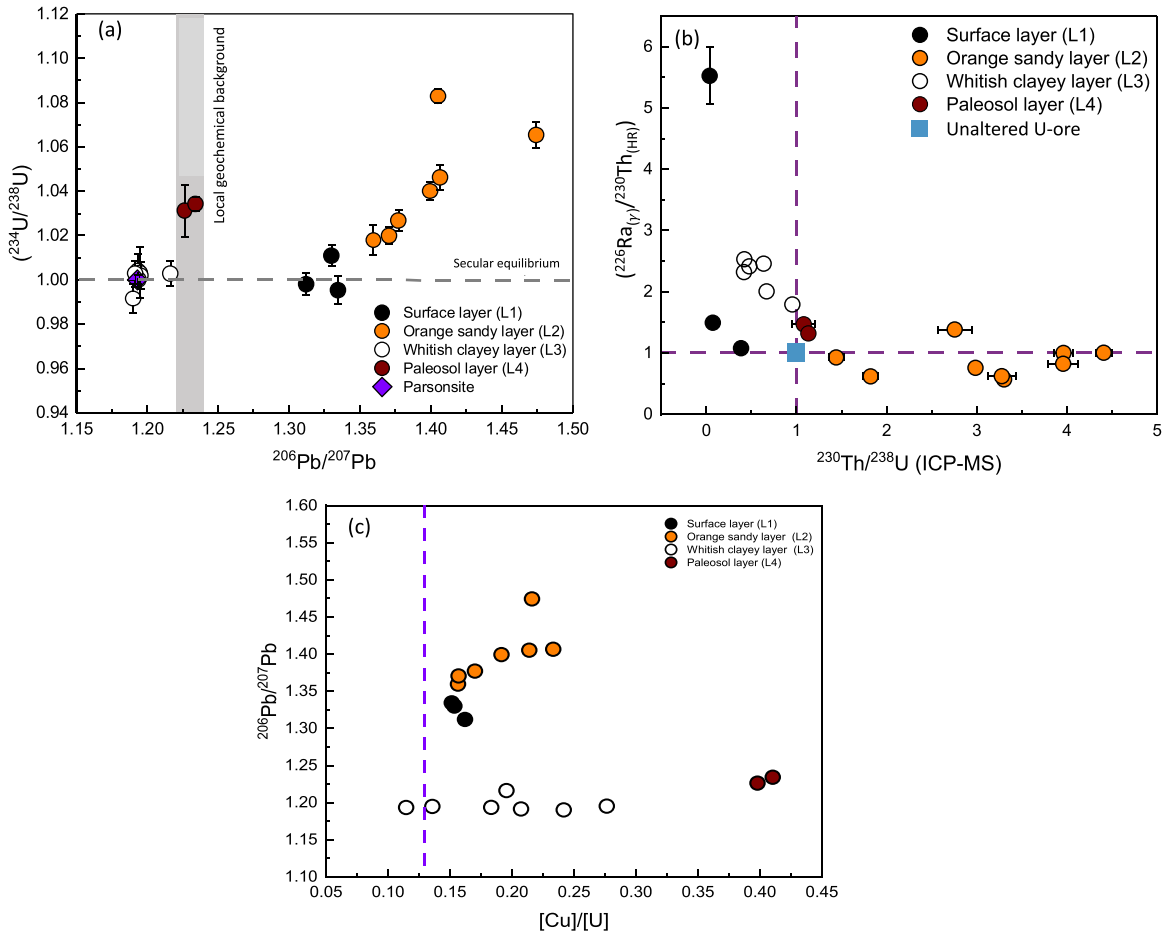

Fig. 8. (a) Pb isotopic ratio ($^{234}U/^{238}U$) vs $^{206}Pb/^{207}Pb$ of different layers in the soil core C5 sampled in the center of the wetland. The dashed line depicts the secular equilibrium value of the ($^{234}U/^{238}U$) activity ratio and the grey field represents the range of $^{206}Pb/^{207}Pb$ ratios corresponding to the local geochemical background. (b) ($^{230}Th/^{238}U$) and ($^{226}Ra/^{230}Th$) activity ratios. The ($^{230}Th/^{238}U$) activity ratios were determined by HR-ICP-MS while the ($^{226}Ra/^{230}Th$) activity ratios were measured by gamma spectrometry. The violet dotted lines represent the secular equilibrium values for each ratio and the blue rectangle represents unaltered U-ore with U-decay products in secular equilibrium. (c) $^{206}Pb/^{207}Pb$ isotope ratio vs concentration ratio of [Cu]/[U] . The dotted line marks the specific [Cu]/[U] ratio (~ 0.13) found in torbernite. When error bars are not visible, they are included within the data points. All uncertainties are expressed with a coverage factor of k=2.

adsorption, complexation onto minerals, organic matter, and colloids, or even coprecipitation with them [25]. The understanding of these deviations and the underlying mechanisms provides essential insights into the mobility and behavior of radionuclides in the environment, with implications for both monitoring and remediation strategies in areas affected by U-mining.

3.3.1. *Whitish clayey layer (L3)*

The whitish clayey layer (L3) displays ($^{230}Th/^{238}U$) activity ratios below 1 (ranging from 0.2 to 0.95) and ($^{226}Ra/^{230}Th$) activity ratios above 1 (ranging from 1.02 to 4.40) (Fig. 6b). This indicates an excess of ^{238}U and ^{226}Ra in this layer. Two transport processes may explain this phenomenon: i) there may have been an input of soluble U and Ra during the mining period or post-deposit, and they were subsequently trapped within this layer and/or ii) redistribution of U/Ra via seasonal fluctuations in the water table.Mobilized U and Ra were accumulated in this layer. The data of other upper layers of L2 and L1 could further highlight the radionuclides mobility in the profile.

3.3.2. *Orange sandy layer (L2)*

Our study unveils a significant disequilibrium in the natural ^{238}U-decay series chain within the orange sandy layer (L2) of all soil cores (Fig. 6b). This disequilibrium, characterized by ($^{230}Th/^{238}U$) activity ratios exceeding 1,could be attributed to three main factors: (i) it could be a consequence of historical U milling activities, wherein ^{238}U was extracted, consequently resulting in a deficiency of ^{238}U and the consequent disequilibrium in the tailings, (ii) the dissolution of U during the transport from mine site to downstream area, (iii) the seasonal fluctuations in the water table level can cause changes in redox conditions, pH, and the chemical composition of pore waters, potentially leading to the dissolution or desorption of U [2,59,60,23,40,56]. SEM analysis revealed the presence of U-bearing phases such as clays and Fe-oxyhydroxides in this layer (Fig. SI-4), supporting the potential for U desorption from these phases. Previous studies have reported significant U resupply from the mine deposit horizon into pore water [23,40]. U-bearing phases without Pb were observed via SIMS (Fig. 9 Area 3), pointing out the neoformation of U-rich particles due to the alteration of primary U-bearing particles and U mobility in the sediment core. Moreover, the observed variations in ($^{226}Ra/^{230}Th$) activity ratios, both exceeding and falling below 1, further imply the potential for inter-mobility of ^{226}Ra within this layer. It may contribute to the accumulation of these elements in layers L1 and L3, while potentially leading to a deficiency of U and Ra in layer L2.

3.3.3. *Surface layer (L1)*

The surface layer (L1) exhibits extremely low ($^{230}Th/^{238}U$) activity ratios, ranging from 0.04 to 0.39, along with ($^{226}Ra/^{230}Th$) activity ratios ranging from 1.05 to 4.32 (Tab. SI-2, SI-5). This is indicative of geochemical processes occurring in U-mining-contaminated wetlands. Notably, the redistribution of U within the organic layer is

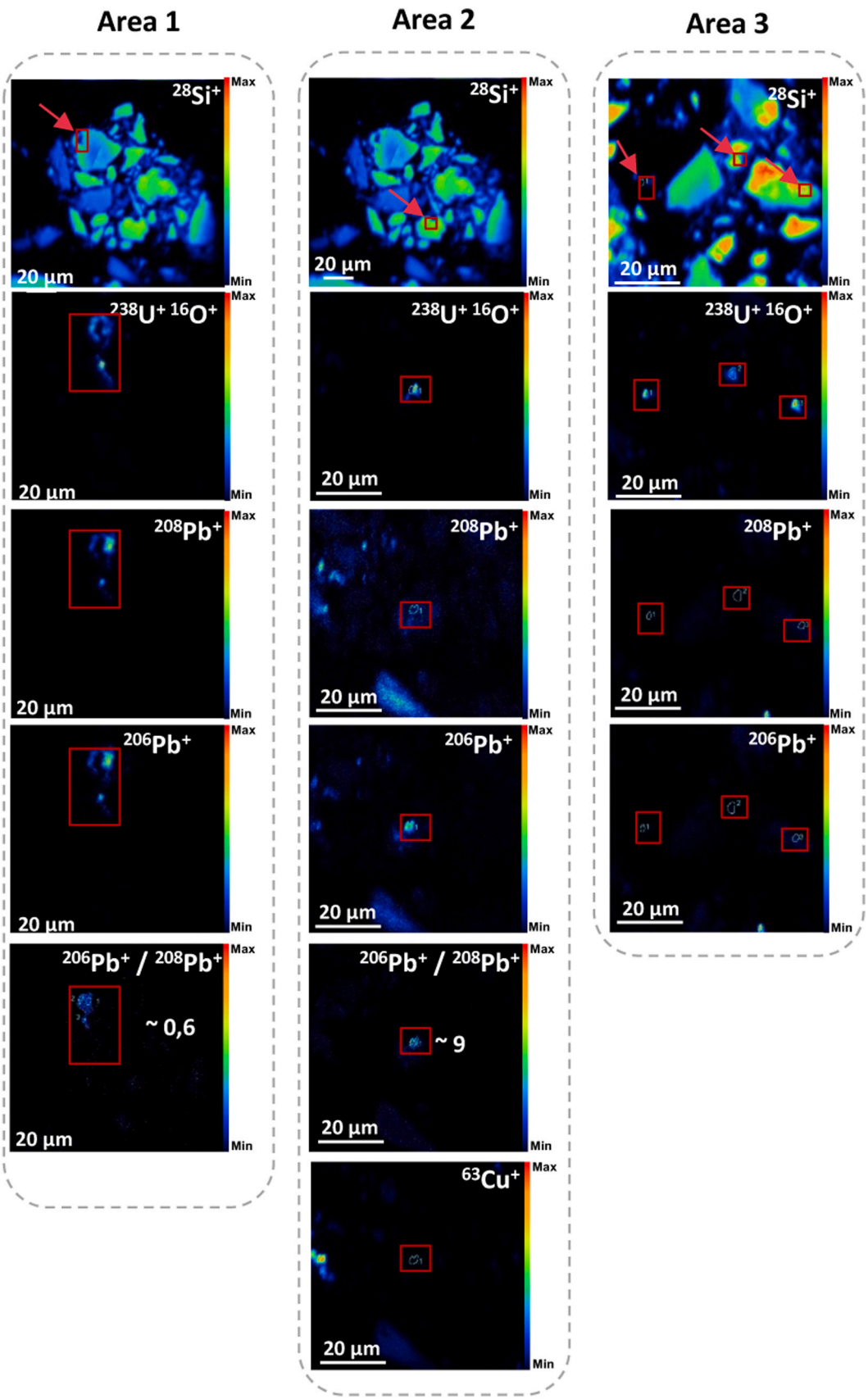

Fig. 9. SIMS mapping of $^{28}Si^{+}$, $^{238}U^{16}O^{+}$, $^{208}Pb^{+}$, $^{206}Pb^{+}$, $^{206}Pb^{+}/^{208}Pb^{+}$ ratio, and $^{63}Cu^{+}$ in three areas containing U-rich particles within the layer L2 of soil core C5 at the depth interval 8.5–9.5 cm. This sample is selected due to its high U and Pb concentration, which can facilitate the localization the U-rich particles observations for SIMS. The identification of U-rich particles displaying radiogenic Pb isotopic ratio serves as additional confirmation of the input of pitchblende from Bois Noirs source in layer L2.

predominantly governed by redox fluctuations and complexation with organic matter, such as carboxyl and phosphoryl groups found in humic substances and microbial biomass [61,6,62,13]. This is underscored by the recent findings of Grangeon et al. [36], which revealed that approximately 63 % of the total U in the surface layer L1 in the downstream wetland of Rophin is bound to organic matter. Moreover, no evident crystalline structure at the nanoscale was observed. This is likely attributed to the prevalent presence of non-crystalline U species firmly bound to organic matter (Fig. SI-5). This is consistent with previous investigations that have studied soils characterized by a high organic content within wetlands [6,45]. In contrast, other mechanisms such as U accumulation via Mn/Fe oxides, U-bearing ore minerals, and uptake by living organisms have been identified as contributing to a lesser extent [22,23,5,7]. In summary, U and Ra could be discharged and transported in both particulate and dissolved forms within the watershed during the mining operations. Subsequently, these elements became trapped in the downstream wetland through mechanisms such as adsorption or coprecipitation onto clay minerals, colloids such as Fe/Mn-oxyhydroxides, and organic matter particles in layers L2 and L3, as supported by previous studies [59,23,56,7]. Furthermore, it is worth noting that fluctuations in the water table level could exert a significant influence on the subsequent redistribution of U and Ra within the soil profile.

4. Conclusion

The results of this work confirmed the substantial radioactive contamination of the Rophin's wetland across various soil layers. Uranium concentrations soared to as high as 14,850 $mg{\cdot}kg^{-1}$, alongside elevated activity levels of ^{226}Ra (up to 35,368 $Bq{\cdot}kg^{-1}$) and ^{230}Th (up to 38,574 $Bq{\cdot}kg^{-1}$). By identifying the origin of the pollution sources, our initial hypothesis of a single contaminated layer resulting from local mining activity has evolved. Another polluted soil layer inherited from the milling activities of U-ore from Bois Noirs mine has been highlighted, where U-ores were transported and processed on the Rophin site. Furthermore, our data offer valuable insights into the mobility of radionuclides within the wetland. The seasonal fluctuations of the water table has been identified as the primary driver of U and ^{226}Ra migration, both in suspended particle and dissolved forms.

This study supports a deeper understanding of the spatiotemporal evolution of radionuclides (U, Ra) in the wetland area. Moreover, this work sheds light on the qualitative functioning of Rophin's wetland, revealing the existence of multiple "reservoirs" containing radioactive elements with distinct physicochemical properties (e.g., parsonsite *vs* pitchblende). This significant discovery will strengthen ongoing research to develop models for the migration of U and ^{226}Ra.

Environmental implications

Even if environmental concerns (ex. wastewater treatment plant) have been integrated in the management plant of the majority of U-mine sites by the operators, in some cases, the mining activities have led to the dissemination of radioactive materials (ex, dust, particles transported through water) in nearby areas. Contaminated sites could cause potential radiological risks to the environment and living organisms. For this reason, this work proposes U-Pb isotopic tracing allowing the efficient identification of these materials in the environment. The identification of these materials can help to address an effective management and remediation strategies for these sites.

CRediT authorship contribution statement

Gilles Montavon: Writing – review & editing, Supervision, Project administration. **Tingting Geng:** Writing – review & editing, Writing – original draft, Validation, Resources, Investigation. **Alkiviadis Gourgiotis:** Writing – review & editing, Validation, Supervision, Project administration, Funding acquisition, Conceptualization. **Arnaud Mangeret:** Writing – review & editing, Validation, Supervision, Resources, Investigation. **Olivier Péron:** Writing – review & editing, Validation, Supervision, Project administration, Funding acquisition. **David Suhard:** Writing – review & editing, Writing – original draft, Resources, Investigation. **Josselin Gorny:** Writing – review & editing. **Louise Darricau:** Writing – review & editing, Resources, Investigation. **Mathieu Le Coz:** Writing – review & editing, Supervision. **Nicolas Aitouabbas:** Writing – review & editing, Resources, Investigation. **Karine David:** Writing – review & editing, Resources, Investigation, Conceptualization. **Christophe Debayle:** Writing – review & editing. **Pascale Blanchart:** Writing – review & editing, Resources, Investigation, Conceptualization.

Declaration of Competing Interest

The authors declare that they have no known competing financial interests or personal relationships that could have appeared to influence the work reported in this paper.

Data Availability

All data are available in supplementary information.

Acknowledgments

We would like to thank the Pays de la Loire doctoral grants, which have co-financed this work. We express our gratitude to Olivier Diez and Cyrielle Jardin for their valuable contribution to the elemental and, isotopic analysis. The authors extend warm thanks to the four reviewers for their constructive comments, which greatly enhanced the article's quality. We also acknowledge the contribution of the IRSN's mass spectrometry platform PATERSON, designated as contribution No. 22.

Appendix A. Supporting information

Supplementary data associated with this article can be found in the online version at doi:10.1016/j.jhazmat.2024.134416.

References

[1] Cuvier, A., Pourcelot, L., Probst, A., Prunier, J., LeRoux, G., 2016. Trace elements and Pb isotopes in soils and sediments impacted by uranium mining. Sci Total Environ 566-567, 238–249. https://doi.org/10.1016/j.scitotenv.2016.04.213. ⟨https://www.sciencedirect.com/science/article/pii/S0048969716309561⟩.

[2] Gourgiotis, A., Mangeret, A., Manhès, G., Blanchart, P., Stetten, L., Morin, G., et al., 2020. New Insights into Pb isotope fingerprinting of U-Mine material dissemination in the environment: Pb isotopes as a memory dissemination tracer. Environ Sci Technol 54, 797–806. https://doi.org/10.1021/acs.est.9b04828 (publisher: American Chemical Society).

[3] Mangeret, A., Blanchart, P., Alcalde, G., Amet, X., Cazala, C., Gallerand, M.O., 2018. An evidence of chemically and physically mediated migration of 238U and its daughter isotopes in the vicinity of a former uranium mine. J Environ Radioact 195, 67–71. https://doi.org/10.1016/j.jenvrad.2018.08.018. ⟨https://www.sciencedirect.com/science/article/pii/S0265931×17310007⟩.

[4] Martin, A., Hassan-Loni, Y., Fichtner, A., Péron, O., David, K., Chardon, P., et al., 2020. An integrated approach combining soil profile, records and tree ring analysis to identify the origin of environmental contamination in a former uranium mine (Rophin, France). Sci Total Environ 747, 141295. https://doi.org/10.1016/j.scitotenv.2020.141295. ⟨https://www.sciencedirect.com/science/article/pii/S0048969720348245⟩.

[5] Schöner, A., Noubactep, C., Büchel, G., Sauter, M., 2009. Geochemistry of natural wetlands in former uranium milling sites (eastern Germany) and implications for uranium retention. Geochemistry 69, 91–107. https://doi.org/10.1016/j.chemer.2007.12.003. ⟨https://linkinghub.elsevier.com/retrieve/pii/S0009281907000554⟩.

[6] Stetten, L., Blanchart, P., Mangeret, A., Lefebvre, P., LePape, P., Brest, J., et al., 2018. Redox fluctuations and organic complexation govern uranium redistribution from U(IV)-phosphate minerals in a mining-polluted wetland soil, brittany, france. Environ Sci Technol 52, 13099–13109. https://doi.org/10.1021/acs.est.8b03031.

[7] Wang, Y., Frutschi, M., Suvorova, E., Phrommavanh, V., Descostes, M., Osman, A.A.A., et al., 2013. Mobile uranium(IV)-bearing colloids in a mining-impacted wetland. Nat Commun 4, 2942. https://doi.org/10.1038/ncomms3942. ⟨https

://www.nature.com/articles/ncomms3942⟩. number: 1 Publisher: Nature Publishing Group.
[8] Taylor, S.R., McLennan, S.M., 1995. The geochemical evolution of the continental crust. Rev Geophys 33, 241–265. https://doi.org/10.1029/95RG00262.
[9] Ivanovich, M., Harmon, R.S., 1992.Uranium-series disequilibrium: applications to earth, marine, and environmental sciences. 2 ed.⟨https://www.osti.gov/etdeweb/biblio/6970644⟩.
[10] Lefebvre, P., 2021.Évolution á long terme de la spéciation et de la mobilité de l'uranium dans les sédiments et les sols: processus naturels d'enrichissement en uranium dans le bassin versant du Lac Nègre. phdthesis. Sorbonne Université.⟨https://theses.hal.science/tel-03680086⟩.
[11] Peña, J., Straub, M., Flury, V., Loup, E., Corcho, J., Steinmann, P., et al., 2020. Origin and stability of uranium accumulation-layers in an Alpine histosol. Sci Total Environ 727, 138368. https://doi.org/10.1016/j.scitotenv.2020.138368. ⟨https://www.sciencedirect.com/science/article/pii/S0048969720318817⟩.
[12] Regenspurg, S., Margot-Roquier, C., Harfouche, M., Froidevaux, P., Steinmann, P., Junier, P., et al., 2010. Speciation of naturally-accumulated uranium in an organic-rich soil of an alpine region (Switzerland). Geochim Et Cosmochim Acta 74, 2082–2098. https://doi.org/10.1016/j.gca.2010.01.007. ⟨https://www.sciencedirect.com/science/article/pii/S0016703710000165⟩.
[13] Wang, Y., Bagnoud, A., Suvorova, E., McGivney, E., Chesaux, L., Phrommavanh, V., et al., 2014. Geochemical control on uranium(IV) mobility in a mining-impacted wetland. Environ Sci Technol 48, 10062–10070. https://doi.org/10.1021/es501556d (publisher: American Chemical Society).
[14] Bollhöfer, A., 2012. Stable lead isotope ratios and metals in freshwater mussels from a uranium mining environment in Australia's wet-dry tropics. Appl Geochem 27, 171–185. https://doi.org/10.1016/j.apgeochem.2011.10.002. ⟨https://www.sciencedirect.com/science/article/pii/S0883292711004227⟩.
[15] Bollhöfer, A., Honeybun, R., Rosman, K., Martin, P., 2006. The lead isotopic composition of dust in the vicinity of a uranium mine in northern Australia and its use for radiation dose assessment. Sci Total Environ 366, 579–589. https://doi.org/10.1016/j.scitotenv.2005.11.016. ⟨https://www.sciencedirect.com/science/article/pii/S0048969705008430⟩.
[16] Santos, R.M., Tassinari, C.C.G., 2012. Different lead sources in an abandoned uranium mine (Urgeiriça - Central Portugal) and its environment impact - isotopic evidence. Geochem Explor Environ Anal 12, 241–252. https://doi.org/10.1144/1467-7873/11-RA-076 (publisher: The Geological Society of London).
[17] Hills, J.H., Richards, J.R., 1976. Pitchblende and galena ages in the Alligator Rivers region, Northern Territory, Australia. Miner Depos 11, 133–154. https://doi.org/10.1007/BF00204477.
[18] Dang, D.H., Wang, W., Pelletier, P., Poulain, A.J., Evans, R.D., 2018. Uranium dispersion from U tailings and mechanisms leading to U accumulation in sediments: Insights from biogeochemical and isotopic approaches. Sci Total Environ 610-611, 880–891. https://doi.org/10.1016/j.scitotenv.2017.08.156. ⟨https://www.sciencedirect.com/science/article/pii/S004896971732154X⟩.
[19] Dickson, B.L., Gulson, B.L., Snelling, A.A., 1985. Evaluation of lead isotopic methods for uranium exploration, Koongarra Area, Northern Territory, Australia. J Geochem Explor 24, 81–102. https://doi.org/10.1016/0375-6742(85)90005-6. ⟨https://www.sciencedirect.com/science/article/pii/0375674285900056⟩.
[20] Peng, B., Chen, H., Fang, X., Xie, S., Wu, S., Jiang, C., et al., 2022. Distribution of Pb isotopes in different chemical fractions in bed sediments from lower reaches of the Xiangjiang River, Hunan province of China. Sci Total Environ 829, 154394. https://doi.org/10.1016/j.scitotenv.2022.154394. ⟨https://www.sciencedirect.com/science/article/pii/S0048969722014875⟩.
[21] Peng, B., Juhasz, A., Fang, X., Jiang, C., Wu, S., Li, X., et al., 2022. Lead isotopic fingerprinting as a tracer to identify the sources of heavy metals in sediments from the Four Rivers' inlets to Dongting Lake, China. CATENA 219, 106594. https://doi.org/10.1016/j.catena.2022.106594. ⟨https://www.sciencedirect.com/science/article/pii/S034181622200580X⟩.
[22] Chautard, C., Beaucaire, C., Gerard, M., Roy, R., Savoye, S., Descostes, M., 2020. Geochemical characterization of uranium mill tailings (Bois Noirs Limouzat, France) highlighting the U and 226Ra retention. J Environ Radioact 218, 106251. https://doi.org/10.1016/j.jenvrad.2020.106251. ⟨https://www.sciencedirect.com/science/article/pii/S0265931×19310045⟩.
[23] Leermakers, M., Phrommavanh, V., Drozdzak, J., Gao, Y., Nos, J., Descostes, M., 2016. DGT as a useful monitoring tool for radionuclides and trace metals in environments impacted by uranium mining: Case study of the Sagnes wetland in France. Chemosphere 155, 142–151. https://doi.org/10.1016/j.chemosphere.2016.03.138.
[24] Siddeeg, M., Bryan, S.D., Livens, N.R.F., 2015. Behaviour and mobility of U and Ra in sediments near an abandoned uranium mine, Cornwall, UK. Environ Sci Process Impacts 17, 235–245. https://doi.org/10.1039/C4EM00230J. ⟨https://pubs.rsc.org/en/content/articlelanding/2015/em/c4em00230j⟩.
[25] Chabaux, F., Riotte, J., Dequincey, O., 2003. U-Th-Ra fractionation during weathering and River Transport. Rev Mineral Geochem 52, 533–576. https://doi.org/10.2113/0520533.
[26] Zielinski, R.A., Bush, C.A., Rosholt, J.N., 1986. Uranium series disequilibrium in a young surficial uranium deposit, northeastern Washington, U.S.A. Appl Geochem 1, 503–511. https://doi.org/10.1016/0883-2927(86)90055-7. ⟨https://www.sciencedirect.com/science/article/pii/0883292786900557⟩.
[27] Regil, E.O., Schleiffer, J.J., Adloff, J.P., Roessler, K., 1989. Chemical effects of α-decay in uranium minerals. Radiochim Acta 47, 177–186. https://doi.org/10.1524/ract.1989.47.4.177 (publisher: De Gruyter (O)).
[28] DePaolo, D.J., Maher, K., Christensen, J.N., McManus, J., 2006. Sediment transport time measured with U-series isotopes: results from ODP North Atlantic drift site 984. Earth Planet Sci Lett 248, 394–410. https://doi.org/10.1016/j.epsl.2006.06.004. ⟨https://www.sciencedirect.com/science/article/pii/S0012821×06004195⟩.
[29] Ng, N.C.W., Li, C., Wang, C., Guo, Y., Duan, Z., Su, N., et al., 2023. A review of global bedrock (234U/238U) disequilibrium and its controlling factors on earth's surface. J Geochem Explor 245, 107144. https://doi.org/10.1016/j.gexplo.2022.107144. ⟨https://www.sciencedirect.com/science/article/pii/S0375674222002023⟩.
[30] Thollon, M., Bayon, G., Toucanne, S., Trinquier, A., Germain, Y., Dosseto, A., 2020. The distribution of (234U/238U) activity ratios in river sediments. Geochim Et Cosmochim Acta 290, 216–234. https://doi.org/10.1016/j.gca.2020.09.007. ⟨https://www.sciencedirect.com/science/article/pii/S0016703720305585⟩.
[31] Sheng, Z., Kuroda, P.K., 1986. Isotopic fractionation of uranium: extremely high enrichments of 234U in the acid-residues of a colorado carnotite. Radiochim Acta 39, 131–138. https://doi.org/10.1524/ract.1986.39.3.131 (publisher: De Gruyter (O)).
[32] Sheng, Z.Z., Kuroda, P.K., 1984. The α-recoil effects of uranium in the Oklo reactor. Nature 312, 535–536. https://doi.org/10.1038/312535a0. ⟨https://www.nature.com/articles/312535a0⟩ (publisher: Nature Publishing Group).
[33] Sheng, Z.Z., Kuroda, P.K., 1986. Further studies on the separation of acid residues with extremely high 234U/238U Ratlos from a Colorado Carnotite. Radiochim Acta 40, 95–102. https://doi.org/10.1524/ract.1986.40.2.95 (publisher: De Gruyter (O)).
[34] Beaumais, A., Mangeret, A., Suhard, D., Blanchart, P., Neji, M., Cazala, C., et al., 2022. Combined u-pb isotopic signatures of u mill tailings from france and gabon: a new potential tracer to assess their fingerprint on the environment. J Hazard Mater 430, 128484. https://doi.org/10.1016/j.jhazmat.2022.128484. ⟨https://linkinghub.elsevier.com/retrieve/pii/S0304389422002722⟩.
[35] Geffroy, J., Sarcia, J.A., Chervet, J., 1960. Les Minerais Uranifères Français Et Leurs Gisements. Institut National Des Sciences Et Techniques Nucléaires, Saclay, France.
[36] Grangeon, S., Roux, C., Lerouge, C., Chardon, P., Beuzeval, R., Montavon, G., et al., 2023. Geochemical and mineralogical characterization of streams and wetlands downstream a former uranium mine (Rophin, France). Appl Geochem, 105586. https://doi.org/10.1016/j.apgeochem.2023.105586. ⟨https://www.sciencedirect.com/science/article/pii/S0883292723000306⟩.
[37] IRSN Mimausa. 2023. Mimausa Web.⟨https://mimausabdd.irsn.fr/⟩.
[38] Himeur, N., 2010.BILAN ENVIRONNEMENTAL Sites miniers du Puy-de-Dôme.
[39] Cuney, M., 1978. Geologic environment, mineralogy, and fluid inclusions of the Bois Noirs-Limouzat uranium vein, Forez, France. Econ Geol 73, 1567–1610. https://doi.org/10.2113/gsecongeo.73.8.1567.
[40] Martin, A., Montavon, G., Landesman, C., 2021. A combined DGT - DET approach for an in situ investigation of uranium resupply from large soil profiles in a wetland impacted by former mining activities. Chemosphere 279, 130526. https://doi.org/10.1016/j.chemosphere.2021.130526. ⟨https://www.sciencedirect.com/science/article/pii/S0045653521009978⟩.
[41] Manhes, G., Allegre, C.J., Provost, A., 1984. U-Th-Pb systematics of the eucrite "Juvinas": precise age determination and evidence for exotic lead. Geochim Et Cosmochim Acta 48, 2247–2264. https://doi.org/10.1016/0016-7037(84)90221-7. ⟨https://www.sciencedirect.com/science/article/pii/0016703784902217⟩.
[42] Millet, M.A., 2007.Interactions de faibles profondeurs et géochimie des basaltes d'îles océaniques: implications sur les modes d'acquisition de la signature isotopique et sur la topogique mantellique. phdthesis. Université Blaise Pascal - Clermont-Ferrand II.⟨https://theses.hal.science/tel-00718419⟩.
[43] Yokoyama, T., Makishima, A., Nakamura, E., 1999. Evaluation of the coprecipitation of incompatible trace elements with fluoride during silicate rock dissolution by acid digestion. Chem Geol 157, 175–187. https://doi.org/10.1016/S0009-2541(98)00206-X. ⟨https://www.sciencedirect.com/science/article/pii/S000925419800206X⟩.
[44] Mangeret, A., Reyss, J.L., Seder-Colomina, M., Stetten, L., Morin, G., Thouvenot, A., et al., 2020. Early diagenesis of radium 226 and radium 228 in lacustrine sediments influenced by former mining sites. J Environ Radioact 222, 106324. https://doi.org/10.1016/j.jenvrad.2020.106324. ⟨https://www.sciencedirect.com/science/article/pii/S0265931×19310203⟩.
[45] Lefebvre, P., LePape, P., Mangeret, A., Gourgiotis, A., Sabatier, P., Louvat, P., et al., 2022. Uranium sorption to organic matter and long-term accumulation in a pristine alpine wetland. Geochim Et Cosmochim Acta 338, 322–346. https://doi.org/10.1016/j.gca.2022.10.018. ⟨https://www.sciencedirect.com/science/article/pii/S0016703722005579⟩.
[46] Branche, G., Chervet, J., Guillemin, C., 1951. Nouvelles espèces uranifères françaises. Bull De Minéralogie 74, 457–488. https://doi.org/10.3406/bulmi.1951.4752. ⟨https://www.persee.fr/doc/bulmi_0037-9328_1951_num_74_7_4752⟩ (publisher: Persée - Portail des revues scientifiques en SHS).
[47] Frostick, A., Bollhöfer, A., Parry, D., 2011. A study of radionuclides, metals and stable lead isotope ratios in sediments and soils in the vicinity of natural U-mineralisation areas in the Northern Territory. J Environ Radioact 102, 911–918. https://doi.org/10.1016/j.jenvrad.2010.04.003. ⟨https://www.sciencedirect.com/science/article/pii/S0265931×1000086X⟩.
[48] Frostick, A., Bollhöfer, A., Parry, D., Munksgaard, N., Evans, K., 2008. Radioactive and radiogenic isotopes in sediments from Cooper Creek, Western Arnhem Land. J Environ Radioact 99, 468–482. https://doi.org/10.1016/j.jenvrad.2007.08.015. ⟨https://www.sciencedirect.com/science/article/pii/S0265931×07002263⟩.
[49] Cathelineau, M., Boiron, M.C., Holliger, P., Poty, B., 1990. Metallogenesis of the French part of the Variscan orogen. Part II: time-space relationships between U, Au and Sn-W ore deposition and geodynamic events — mineralogical and U-Pb data. Tectonophysics 177, 59–79. https://doi.org/10.1016/0040-1951(90)90274-C. ⟨https://www.sciencedirect.com/science/article/pii/004019519090274C⟩.

[50] Schoene, B., 2014. 4.10 - U-Th-Pb Geochronology. In: Holland, H.D., Turekian, K.K. (Eds.), Treatise on Geochemistry, Second edition.,. Elsevier, Oxford, pp. 341–378. ⟨https://www.sciencedirect.com/science/article/pii/B9780080959757003107⟩. 10.1016/B978-0-08-095975-7.00310-7.
[51] Cumming, G.L., Richards, J.R., 1975. Ore lead isotope ratios in a continuously changing earth. Earth Planet Sci Lett 28, 155–171. https://doi.org/10.1016/0012-821X(75)90223-X. ⟨https://www.sciencedirect.com/science/article/pii/0012821×7590223X⟩.
[52] Liu, J., Luo, X., Wang, J., Xiao, T., Yin, M., Belshaw, N.S., et al., 2018. Provenance of uranium in a sediment core from a natural reservoir, South China: application of Pb stable isotope analysis. Chemosphere 193, 1172–1180. https://doi.org/10.1016/j.chemosphere.2017.11.131. ⟨https://www.sciencedirect.com/science/article/pii/S0045653517319082⟩.
[53] Mathuthu, M., Khumalo, N., 2018. Determination of lead isotope ratios in uranium mine products in South Africa by means of inductively coupled plasma mass spectrometry. J Radioanal Nucl Chem 315, 1–12. https://doi.org/10.1007/s10967-017-5641-z.
[54] Lowson, R., Short, S., 1986.234U/238U and 230Th/234Uactivity ratios in mineral phases of a lateritic weathered zone.
[55] Gulson, B.L., Mizon, K.J., Korsch, M.J., Noller, B.N., 1989. Lead isotopes as seepage indicators around a uranium tailings dam. Environ Sci Technol 23, 290–294. https://doi.org/10.1021/es00180a004.
[56] Meyer-Georg, S., 2021.Étude de la spéciation et de la mobilité de l′uranium(VI) dans les eaux naturelles: effet des matières organiques. phdthesis. Université de Strasbourg.⟨https://theses.hal.science/tel-03649417⟩.
[57] Bister, S., Birkhan, J., Lüllau, T., Bunka, M., Solle, A., Stieghorst, C., et al., 2015. Impact of former uranium mining activities on the floodplains of the Mulde River, Saxony, Germany. J Environ Radioact 144, 21–31. https://doi.org/10.1016/j.jenvrad.2015.02.024. ⟨https://www.sciencedirect.com/science/article/pii/S0265931×15000600⟩.
[58] Dequincey, O., Chabaux, F., Clauer, N., Sigmarsson, O., Liewig, N., Leprun, J.C., 2002. Chemical mobilizations in laterites: evidence from trace elements and 238U-234U-230Th disequilibria. Geochim Et Cosmochim Acta 66, 1197–1210. https://doi.org/10.1016/S0016-7037(01)00845-6. ⟨https://www.sciencedirect.com/science/article/pii/S0016703701008456⟩.
[59] Husson, A., Leermakers, M., Descostes, M., Lagneau, V., 2019. Environmental geochemistry and bioaccumulation/bioavailability of uranium in a post-mining context - the Bois-Noirs Limouzat mine (France). Chemosphere 236, 124341. https://doi.org/10.1016/j.chemosphere.2019.124341. ⟨https://www.sciencedirect.com/science/article/pii/S0045653519315589⟩.
[60] LePape, P., Stetten, L., Hunault, M.O., Mangeret, A., Brest, J., Boulliard, J.C., et al., 2020. HERFD-XANES spectroscopy at the U M-edge applied to the analysis of U oxidation state in a heavily contaminated wetland soil. Appl Geochem 122, 104714. https://doi.org/10.1016/j.apgeochem.2020.104714. ⟨https://linkinghub.elsevier.com/retrieve/pii/S0883292720302067⟩.
[61] Mitchell, N., Pérez-Sánchez, D., Thorne, M.C., 2013. A review of the behaviour of U-238 series radionuclides in soils and plants. J Radiol Prot 33, R17. https://doi.org/10.1088/0952-4746/33/2/R17.
[62] Stetten, L., Lefebvre, P., LePape, P., Mangeret, A., Blanchart, P., Merrot, P., et al., 2020. Experimental redox transformations of uranium phosphate minerals and mononuclear species in a contaminated wetland. J Hazard Mater 384, 121362. https://doi.org/10.1016/j.jhazmat.2019.121362. ⟨https://www.sciencedirect.com/science/article/pii/S0304389419313160⟩.